Dielectric breakdown in media with defects

Jeffrey Boksiner and P. L. Leath
Department of Physics and Astronomy, Rutgers University, Piscataway, New Jersey 08855-0849
(Received 18 August 1997)

We investigate the breakdown field and geometry of breakdown paths of an electrical circuit model for dielectric breakdown in media with defects of arbitrary residual resistivity. The circuit model consists of a two-dimensional square lattice network of resistors that break down from a high resistance to a lower (residual) resistance when the local electric field exceeds a critical value. We consider infinite and semi-infinite samples with a single cluster (needle) of defects as well as samples with a finite concentration of defects from the dilute limit to the percolation threshold. We find that for needle defects with nonzero residual resistivity, the breakdown field reaches a finite value as the defects lengthen, causing the random lattice to reach the same breakdown field in the thermodynamic limit. Furthermore, we find that depending on the initial length of the seed defect and the residual resistivity, the breakdown either grows one dimensionally, or spreads with a fractal dimension. We give the phase diagram and relevant exponents for this crossover, and report similar behavior in random lattices at dilute defect concentrations. [S1063-651X(98)03103-1]

PACS number(s): 41.20.Cv, 03.50.De, 77.22.Jp, 64.60.Cn

I. INTRODUCTION

Random nonlinear resistor and fuse networks provide realistic and tractable models for understanding the geometry and stability of dielectric breakdown and other breakdown phenomena [1,2]. Although the random-fuse network, and its dual in two dimensions, the random nonlinear resistor network, have been studied extensively [3–7], few studies have investigated breakdown models where the broken bonds have nonzero resistivity (residual resistivity) [5]. Since dielectric breakdown of real materials results in nonzero resistivity, its effect is an important consideration.

In this paper we investigate the breakdown field and the geometry of breakdown paths of an electrical circuit model for dielectric breakdown in media with defects of arbitrary residual resistivity. Previous studies of random networks have shown that, in dilute samples, the breakdown process begins at the critical defect in the network. The critical defect for dielectric breakdown is often a long thin defect — a needle directed along the electric field. Characteristics of the breakdown process on a random lattice, including the breakdown field and the geometry of the breakdown cluster, are related to the characteristics of the breakdown for the needle defect. Few studies have examined the nature of the needle growth in detail; although, in one of the first studies, Takayasu observed that breakdown clusters usually have similar shape [8]. The clusters in that study exhibited bifurcation, i.e., the spreading of breakdown paths into two dimensions, but a definitive cause was not identified.

We are interested in the breakdown field as a function of residual resistivity, and in examining the geometrical structure of the breakdown cluster in order to separate the aspects of the structure inherent in the growth of needles in homogeneous media from those arising from the disorder in the system. We simulated such growth on two-dimensional square lattice networks. Unfortunately, a study of needle growth requires simulations on large and computationally expensive lattices. So, to perform our study, we developed a new algorithm, described in Appendix A, that uses Green's functions to compute the field due to a collection of defects in an infinite homogeneous medium exactly. In Sec. II A we investigate the fields due to the presence of needle defects in a homogeneous medium, using analytical and numerical methods. In Sec. II B, we report on simulations of needle growth in homogeneous media. In Secs. III A and III B we use these results to analyze the breakdown field and paths on random lattices. Finally, in Sec. III C we report on the numerical simulation of breakdown on disordered lattices.

Breakdown process

We need to define the rules used in simulation carefully, since differences in the simulation can lead to different results for needle growth. Our adiabatic simulation of the breakdown growth proceeds as follows. The initial defect configuration is selected. Each defect is a bond of residual resistance $R_b<1$ in an infinite or semi-infinite two-dimensional square lattice of 1-Ω resistors, as shown in Fig. 1. A uniform electric field is applied to the lattice along the vertical crystalline axis. The field magnitude is determined by its value in a region far from the defects for the infinite lattice, or by the applied voltage for a finite lattice. All bonds

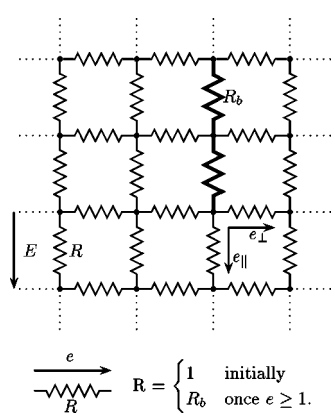

FIG. 1. A section of an infinite lattice of resistors with a two-defect needle (heavy line) oriented along the direction of the applied field.

where the local field exceeds the critical field, taken to be unity, break down, becoming defects and lowering their resistance to R_b irreversibly. The local fields are recalculated for the new configuration of defects, and the process is repeated. Note that it is always possible to rescale resistances and the electric fields so that the resistances of the lattice and the critical field are unity. This simulation allows for an extension of the random-resistor network to an infinite lattice; it is different from the dielectric breakdown model (DBM) of Pietronero and Evertsz [9]. The main difference is that, for deterministic breakdown, the DBM causes breakdown only in a single branch for each iteration, which produces a qualitatively different geometry of needle growth.

II. NEEDLE DEFECTS ON A HOMOGENEOUS LATTICE

We investigate the growth of a needle defect (a chain of l_0 nearest-neighbor defects of resistance R_b oriented along the applied field) in an otherwise homogeneous infinite lattice. There are three independent parameters: the initial defect length l_0, the magnitude of the applied field E, and the residual resistance of the defect resistor R_b. We found that, depending on the parameters, needle growth exhibits a behavior that corresponds to one of three phases of the breakdown process. The lattice is in the insulating phase (there is no connected path of defects across the lattice) if the applied field is too small to initiate breakdown. As the field increases, it reaches a critical value, which we call the initial breakdown field E_{bi}, that just initiates breakdown and causes the needle defect to grow through the lattice. Depending on the initial parameters, the breakdown may proceed in a single path or in a fractal tree, as Sec. II B shows.

A. Breakdown field

As the field is applied, the local field is greatest at the tip of the needle (of length l_0), causing breakdown growth to begin there. This happens when $e_{\parallel}(E)=1$. For $R_b=0$, an analytic calculation of the tip fields presented in Appendix B 3 gives

$$e_{\parallel}\simeq E\left(1.132\sqrt{2l_0}+\frac{0.218}{\sqrt{2l_0}}\right), \tag{1a}$$

$$e_{\perp}\simeq E\left(0.8\sqrt{2l_0}-\frac{0.154}{\sqrt{2l_0}}\right). \tag{1b}$$

This shows that the tip field increases without limit as $\sqrt{l_0}$, causing the initial breakdown field E_{bi} to go to zero as $l_0^{-1/2}$. Unfortunately, we have not been able to obtain exact analytic results on square lattices for needles of nonzero residual resistivity. Considerations of elliptical defects in continuous media, presented in Appendix B, suggest that the tip fields reach a finite asymptotic value for long defects. We calculated the fields numerically using the algorithm of Appendix A. Typical field behavior is shown in Fig. 2. As expected, the fields appear to approach an asymptotic value. The numerically calculated asymptotic fields appear in Fig. 3.

In all cases, the tip field increases with needle length, so that, once the needle begins to grow, it cannot stop, i.e., the system is brittle. Thus the final breakdown field for the system is equal to the initial breakdown field, $E_b=E_{\mathrm{bi}}$. Section II B examines needle growth in more detail.

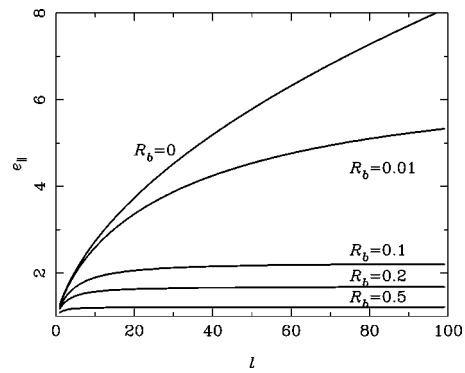

FIG. 2. The field at the tip of the needle $e_{\parallel}$ vs needle length l for various R_b at $E=1$. The fields e_l and E are in units of breakdown field of individual resistors, l is in units of lattice spacing, and R_b is the ratio of resistance after breakdown to resistance before breakdown.

B. Breakdown paths

We studied the path formed by the broken bonds. The needle begins to grow at $E=E_{\mathrm{bi}}$. At first, the growth consists of elongation of the needle so that the defect remains one dimensional (1D), but, for defects with low residual resistance, the needle bifurcates as it grows longer, spreading two dimensionally, and spans a finite sector of the medium. Figure 4 shows growth patterns for four different configurations. Figure 5 shows a graph used to measure the fractal dimension D of the patterns using the procedure of counting the number of filled boxes at various scales [10,11]. The points below the line illustrate finite lattice effects. Excluding these, the four patterns exhibit a fractal dimension $D=1.722\pm0.018$.

As R_b increases, the onset of 2D growth occurs at longer needles, and requires more iterations until, at a certain critical residual resistance, the growth is purely one dimensional as the needle never bifurcates. However, at higher applied fields, the transition from 1D to 2D growth occurs at larger

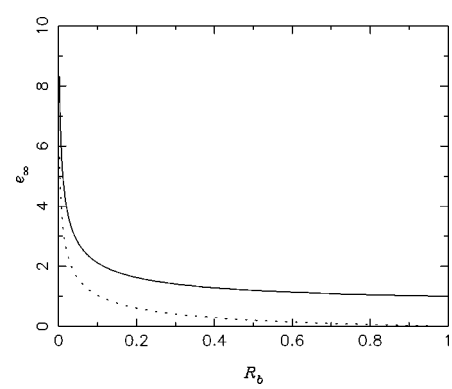

FIG. 3. The asymptotic values of the field, for $l\rightarrow\infty$, at the tip of the needle – $e_{\parallel\infty}$ (solid line) and $e_{\perp\infty}$ (dotted line) vs R_b at $E=1$. The fields e_{∞} are in the units of the breakdown field of individual resistors, and R_b is the ratio of resistance after breakdown to resistance before breakdown.

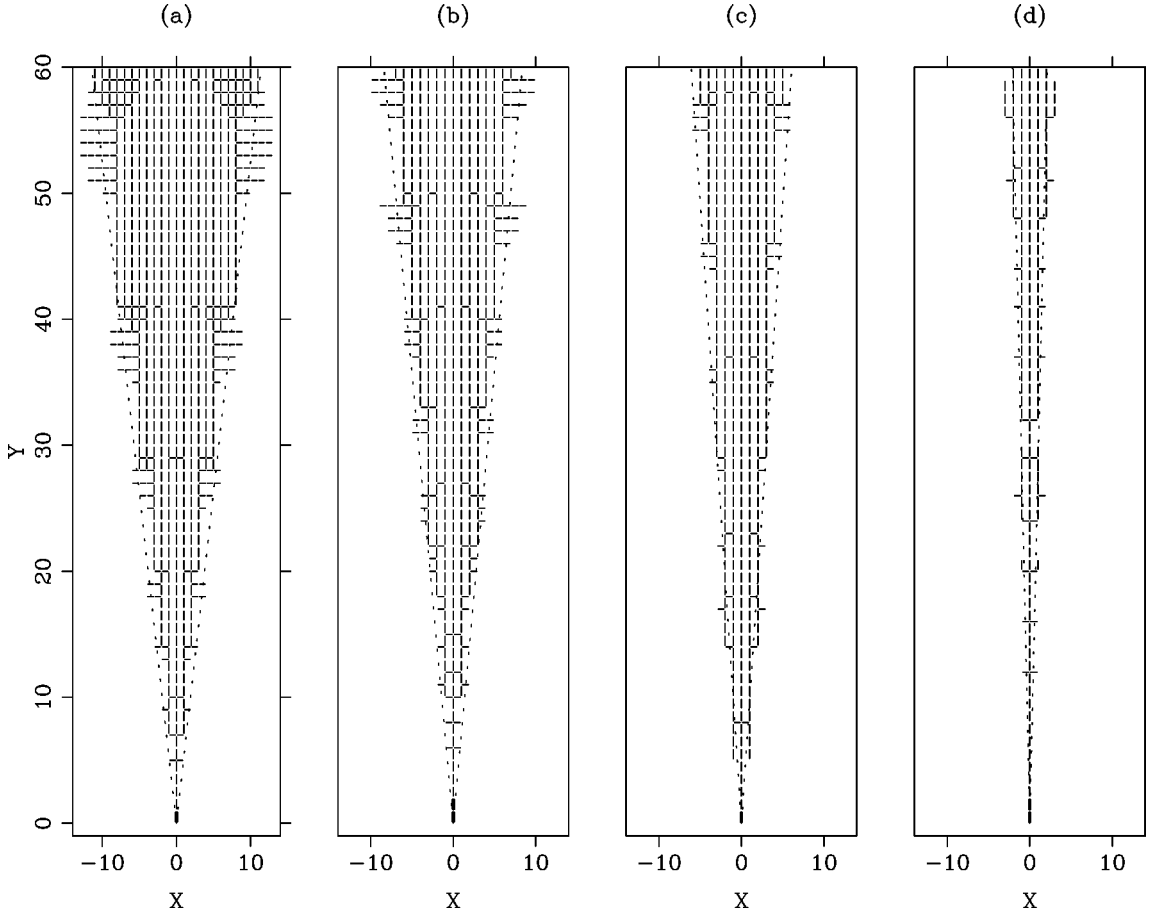

FIG. 4. Growth clusters for four configurations on the semi-infinite lattice: (a) $R_b=0$, $l_0=2$; (b) $R_b=0$, $l_0=4$; (c) $R_b=0.03$, $l_0=2$; (d) $R_b=0.03$, $l_0=4$. The axes X and Y denote the number of lattice spaces in each direction. The thick lines are the initial defects, the thin dashed lines are the broken-down bonds, and the dotted lines outline the angle filled out by the growing cluster.

values of R_b. When the applied field reaches unity, the whole lattice breaks, so that there is 2D growth for all values of R_b.

Thus the lattice can exist in three distinct states: insulating, 1D breakdown, or 2D breakdown (referring to topological dimension, i.e., within a 2D wedge). To obtain a qualitative understanding of this behavior, we studied the fields at the tip of an elliptical defect. The results are described in Appendix B.

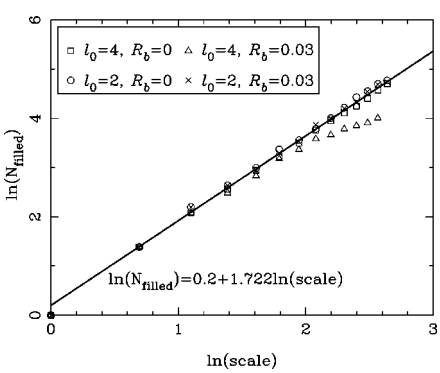

FIG. 5. Graph of the logarithm of the number of occupied boxes vs the logarithm of the scale of the linear size of each box when the cluster is covered by a mesh of boxes. l_0 is in units of the lattice spacing. R_b is the ratio of resistance after breakdown to resistance before breakdown.

For zero-resistance defects, the fields at the tip grow without bounds as the needle elongates. Thus, if we have a defect at the initial breakdown field, the adjacent bond breaks down, the cluster elongates, and the tip field becomes even stronger, causing the defect to grow without limit. But, as the defect grows, the field perpendicular to the cluster axis also grows, leading to the eventual failure of horizontal bonds as well, causing the defect to spread out and become greater than one dimensional. We see that zero-resistance defects always eventually spread in two dimensions.

However, for defects with nonzero residual resistivity, the fields at the tip reach an asymptotic value. Thus the defect elongates as before, but the perpendicular field may or may not reach unity. If $e_{\perp\infty}(E)\geqslant 1$ the defect bifurcates, but if $e_{\perp\infty}(E)<1$, the defect cluster stays one dimensional as it grows.

C. Numerical simulation of the phase behavior

Armed with this understanding, we can now construct a phase diagram. We calculate the asymptotic field on an infinite lattice numerically for different R_b, and we calculate $E_{\rm bi}$ for different R_b and l_0. Thus we determine whether the needle bifurcates for each configuration. The phase diagram is shown in Fig. 6. The bottom sheet corresponds to $E_{\rm bi}$, while the top sheet corresponds to the field required to produce ''spreading'' breakdown. Where the two sheets merge, the breakdown paths are always more than one dimensional.

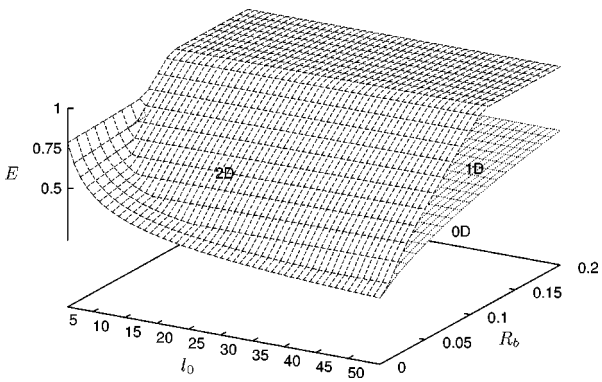

FIG. 6. Phase surface for needle growth. E is in the units of breakdown field of individual resistors. l_0 is in the units of lattice spacing. R_b is the ratio of resistance after breakdown to resistance before breakdown.

Figure 7 shows the phase diagram at $E=E_{\rm bi}$. The line separating 1D and 2D regions corresponds to the line where the two sheets join in Fig. 6. This phase boundary, for l_0 vs $1/R_b$ is approximately a straight line $l_0 \cong a/R_0 - b$, where $a = 0.44 \pm 0.002$ and $b = 3.96 \pm 0.14$.

We also numerically studied the length $l_{\rm bi}$ that the needle reaches prior to bifurcation for various R_b and l_0 at $E=E_{\rm bi}$. Figure 8 shows the results. As R_b approaches the critical value at a particular $l_0, l_{\rm bi}$ diverges. We attempted to fit these curves to a power law of the form

$$l_{\rm bi} = a(b-R_b)^{-c}. \tag{2}$$

The resulting fits are excellent for all values of l_0. The sample of exponents has a median of 0.745, and a standard deviation of 0.038. These results are consistent with an exponent of 0.75.

III. DISORDERED LATTICE

In Sec. II we considered the initial breakdown field and the growth patterns on a perfect infinite or semi-infinite lattice with a single needle defect. In this section we investigate the effect of residual resistance on the breakdown properties of a square $N \times N$ disordered lattice with periodic boundary conditions. The disorder comprises a fraction p of bonds that randomly have an initial resistance of R_b, i.e., initially, a fraction p of bonds is broken down randomly. There are three parameters, N, p, and R_b, and the applied field E

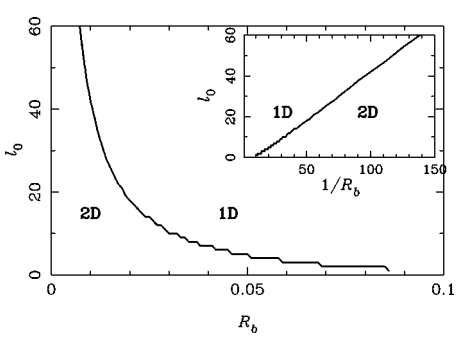

FIG. 7. Phase diagram for needle growth at the critical field. l_0 is in units of the lattice spacing, R_b is the ratio of resistance after breakdown to resistance before breakdown.

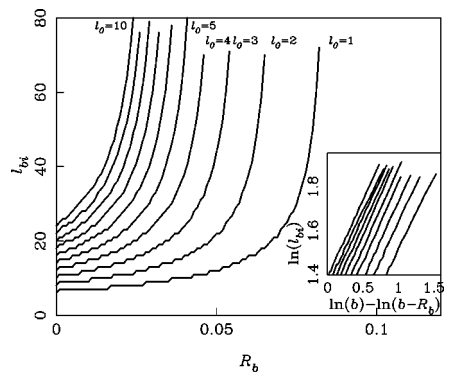

FIG. 8. Needle length at bifurcation $l_{\rm bi}$ as a function of R_b for $E=E_{\rm bi}$ for all values of l_0 between 1 and 10. The inset shows $l_{\rm bi}$ vs $(b-R_b)$ on a log-log scale. The offset b was calculated using a fit of a, b, and c to Eq. (2) for each value of l_0. The curves from right to left in both figures correspond to increasing values of l_0. The lengths l_0 and $l_{\rm bi}$ are in the units of the lattice spacing, and R_b is the ratio of resistance after breakdown to resistance before breakdown.

$=V/N$, where V is the applied voltage. We study the effect of residual resistance on the breakdown field and the breakdown paths.

One difficulty in looking at a lattice with non-zero-resistivity defects is that, for large R_b, the presence of a spanning breakdown cluster does not necessarily change the overall lattice resistance significantly. Thus we define breakdown geometrically—breakdown is deemed to have occurred when there is a cluster of defects spanning the entire lattice.

A. Breakdown voltage

To investigate the properties of the breakdown field, we consider the lattice in the dilute limit $p \ll 1$ and the limit near the percolation transition $p \sim p_c = 0.5$. We also investigate the breakdown field numerically for all p.

1. Dilute limit

In the dilute limit, the initial breakdown voltage is controlled by the probability of the occurrence of critical defects [2]. The probability that a needle of length l occurs in an $N \times N$ lattice is on the order of $p^l N^2$. The value l producing a probability of order 1 corresponds to the length l_c of the characteristic largest defect cluster on such a lattice,

$$l_c \sim -\frac{2 \ln N}{\ln p}. \tag{3}$$

We expect the breakdown field to be controlled by the field enhancement at the tip of such a defect cluster, so that

$$E_{\rm bi} \simeq \frac{1}{e_{\parallel}(l_c, R_b)}. \tag{4}$$

For a lattice with zero-resistance defects the field behaves according to Eq. (1) as $\sim \sqrt{l_c}$, which leads to the logarithmic vanishing of the breakdown field with the increase in lattice size reported previously [3]. However, with non-zero-resistance defects, the field at the tip reaches the limiting value shown in Fig. 3, so that, beyond some critical lattice

size, the breakdown field is finite and independent of the sample size. In the thermodynamic limit $N\to\infty$, as p changes from zero, we expect a rather sharp transition of the breakdown field from unity to the inverse of the value shown in Fig. 3.

At larger p we expect $E_{\rm bi}$ to decrease due to the increased probability of configurations with a small gap between elongated defects. Such configurations have a smaller initial breakdown voltage, but the breakdown may not be sustainable [5]. Instead, the result is a single elongated defect, whose breakdown field is given by the inverse of $e_{\|\infty}$. Thus we expect $E_b \simeq 1/e_{\|\infty}$ even beyond the dilute region.

2. Near the percolation transition

Near the critical percolation threshold p_c, the breakdown field is controlled by the largest defect cluster in the network, whose linear size is of order N. If the cluster percolates (spans the entire lattice), the breakdown strength is zero identically. Otherwise, the largest cluster is nearly percolating except for a small number x of bonds that need to be broken. These single ''red'' gap bonds are the dual of ''red'' bonds of the random-fuse network. The breakdown strength of the lattice depends upon the breakdown strength of the gap $E_{\rm bg}(x)$, which fluctuates for the same x depending on the configuration. The average size of the gap depends on p so that the average breakdown field $\langle E_b\rangle$ is $\langle E_{\rm bg}(x)x(p,N)\rangle$. However, we expect that the fluctuations of the gap breakdown field are small for small gaps, so we can characterize the gap breakdown field by a single-parameter function $E_{\rm bg}(x)$, which is configuration independent for a given x.

For a finite-size lattice, we can define p_c to occur where the probability of a spanning cluster is $\frac{1}{2}$. The dominant configurations near p_c are those with either a percolating cluster or an almost percolating cluster with a single red gap bond. Hence we can approximate the average breakdown field near the critical point by assuming that there are only those two states,

$$\langle E_b\rangle \simeq E_{\rm bg}(1)[1-P(p,N)], \tag{5}$$

where $P(p,N)$ is the probability that a percolating cluster occurs. This relation allows us to relate the breakdown field to $P(p,N)$ whose properties have been investigated extensively [10]. We can, for simplicity, estimate $E_{\rm bg}(1)$ by considering a cluster that spans the lattice except for the bottommost row. We assume that the bottommost row contains unity resistances only, while the top $N-1$ rows are composed of uniform medium of effective resistance R_m. By translational symmetry, the field across the gap is found by voltage division as $\{1/[1+R_m(N-1)]\}NE$. Breakdown occurs when the field across the gap is unity, so that $1=\{1/[1+R_m(N-1)]\}NE_{\rm bg}(1)$, leading to

$$E_{\rm bg}(1)=\frac{1+R_m(N-1)}{N}\sim R_m. \tag{6}$$

An effective medium theory is appropriate because the resistance of the percolating cluster is $\sim R_b N^{\mu/\nu}$, with $\mu/\nu=0.975$ in two dimensions, where μ is the conductivity exponent and ν the correlation-length exponent. This resistance increases without bound for large N, while the total resistance of the lattice cannot exceed unity. Hence, for sufficiently large N, the overall medium dominates the resistance.

The expression for the resistance of the effective medium was presented by Kirkpatrick [12]. For two dimensions it is

$$R_m=\frac{2p-1+R_b(1-2p)}{2}+\frac{\sqrt{[2p-1+R_b(1-2p)]^2+4R_b}}{2}. \tag{7}$$

At $p=\frac{1}{2}$, $R_m=\sqrt{R_b}$, so that

$$E_{\rm bg}(1)\simeq\sqrt{R_b}. \tag{8}$$

Thus the breakdown field at p_c can be approximated by substituting Eqs. (8) and (6) into Eq. (5),

$$\langle E_b\rangle \simeq \frac{1+\sqrt{R_b}(N-1)}{N}[1-P(p,N)]\sim\sqrt{R_b}[1-P(p,N)]. \tag{9}$$

This grossly simplified argument suggests that the breakdown strength of a large system with a single red bond with nonzero residual resistivity remains finite as the lattice size increases. Physically, this is reasonable, since for $R_b=0$ the entire applied voltage appears across the red bond, causing its breakdown strength to decrease as $1/N$, while for nonzero resistivity defects, the field dissipates in the defects.

Looking at Eq. (9), $P(p,N)$ undergoes a sharp transition near p_c from nearly zero to nearly unity [10]. This transition occurs over a region of width Δ_p, where $\Delta_p\sim N^{-1/\nu}$ and $\nu=\frac{4}{3}$ in two dimensions. This implies that E_b undergoes a sharp transition to a breakdown strength of essentially zero, regardless of R_b.

In the thermodynamic limit, at any $p<p_c$, the lattice size is always larger than the largest cluster, so that the dilute behavior prevails up until the transition. The transition approaches a step function, and therefore we expect the breakdown field to make a sharp transition from $1/[e_{\|\infty}(R_b)]$ to zero. Thus we expect a disordered lattice in the thermodynamic limit $N\to\infty$ to have three phases as function of p,

$$E_b=\begin{cases} 1 & \text{if } p=0,\\ \dfrac{1}{e_{\|\infty}(R_b)} & \text{if } 0<p<p_c\\ 0 & \text{if } p\geqslant p_c. \end{cases} \tag{10}$$

B. Breakdown paths

We also expect the nature of breakdown paths in the disordered lattices to vary with p. In the dilute limit we expect the paths to originate at the critical defects and grow in a manner similar to that of a needle on an infinite, perfect square lattice. The fractal dimension of such paths should be about 1.722 if l_c is in the 2D region of Fig. 7, and close to unity if l_c is in the 1D region. This implies, that we expect the fractal dimension of the breakdown cluster at some p to decrease as l_c increases or N increases [as given by Eq. (3)] or R_b increases.

Near the percolation transition, we expect the geometrical properties of the breakdown cluster to be controlled by the percolation process, and to be given by the largest defect

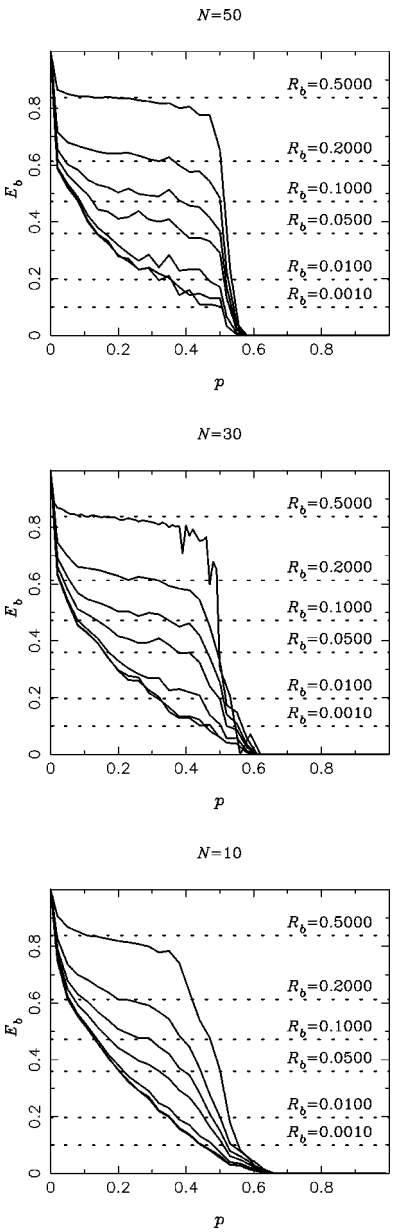

FIG. 9. E_b vs p at various R_b plotted for three lattice sizes N. E_b is in the units of breakdown field of individual resistors. Each point is averaged over 50 configurations for $N=10$ and ten configurations for $N=30$ and 50. The dotted line represents $1/e_{\|\infty}(R_b)$.

cluster that exists prior to breakdown. The number of local breakdowns required to achieve total breakdown of the lattice is very small, so we expect that all breakdown clusters at $p \sim p_c$ will have fractal dimension of the percolating cluster ($D \simeq 1.905$) [10] regardless of residual resistivity.

C. Numerical results

We investigated the breakdown on an $N \times N$ square lattice with periodic boundary conditions using Monte Carlo simulations. Our computer program solved the circuit using nodal analysis, with the admittance matrix inverted using the conjugate-gradient method [13]. The program performed simulations at $N=10$, 20, 30, 40, and 50 and $R_b=0.0001$, 0.001, 0.01, 0.1, 0.2, and 0.5. For each lattice size, p was

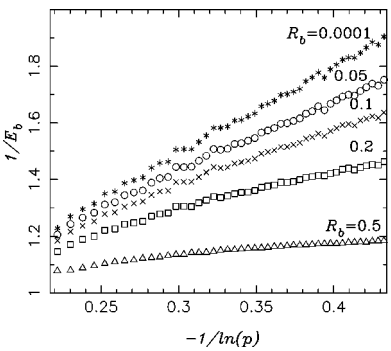

FIG. 10. $1/E_b$ vs $-1/\ln(p)$ in the dilute limit. E_b is in the units of breakdown field of individual resistors. There are 5000 simulations at each point.

swept in increments of 0.03 starting at $p=0.02$. Ten samples at each parameter point were simulated at $N>10$, while 50 realizations were simulated at $N=10$. The programs were run on the IBM SP2 supercomputer at the Cornell theory center using message passing interface (MPI) [14] for parallel coding.

1. Breakdown voltage

Figure 9 shows the breakdown field averaged over random initial configurations as a function of concentration of initial defects p on three different lattice sizes at different R_b. Ten configurations for each data point were averaged for $N=30$ and 50, and 50 configurations for $N=10$. Dashed lines indicated the values expected from the asymptotic form [Eq. (10)], at intermediate concentrations p. Lattices with large R_b reach the asymptotic value quickly because their respective needles rapidly reach their asymptotic values. Lattices with small R_b require large N to reach this value.

Figure 10 shows the inverse of the breakdown field $1/E_b$ as a function of $-1/\ln(p)$ at the dilute limit for 10×10 lattice averaged over 5000 simulations for each point. The curves of Fig. 10 are consistent with Eq. (3), Eq. (4), and the curves of Fig. 2.

2. Near the percolation transition

We tested our assumption that the breakdown field near the percolation transition is proportional to the probability of occurrence of a percolating cluster $P(p,N)$, as given by Eq. (5). We performed 10 000 simulations on 10×10 lattice at $R_b=0.1$ and 0.5 for $0.4<p<0.6$. We measured from the simulations the breakdown field E_b and the percolation probability $P(p,N)$ (the probability of spanning the sample). Then we plotted the breakdown field as a function $P(p,N)$ in Fig. 11. A linear curve fit yielded the values of $E_{\rm bg}(1)$, which were 0.41 at $R_b=0.1$ and 0.76 at $R_b=0.5$. This agrees well with Eq. (6), which predicts $E_{\rm bg}(1)$ of 0.44 and 0.74 for a 10×10 lattice. Thus on a small lattice we were able to verify Eq. (8), which gives us information about the approach to the critical point, such as the critical exponent, while large lattices are necessary to study such properties directly.

3. Breakdown paths

Figures 12–14 show the breakdown paths for three different initial parameters. As expected, the paths are straight for

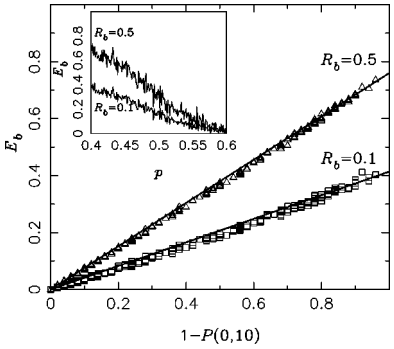

FIG. 11. E_b vs $P(p,N=10)$ at R_b of 0.1 and 0.5 for $0.4 \leqslant p \leqslant 0.6$. The solid lines represent linear curve fits to the points. The inset shows a curve of E_b vs p using the same data. E_b is in units of the breakdown field of individual resistors.

large R_b and spread out for small R_b. In Fig. 15 we plot the fractal dimension as a function of p for two extreme values of R_b. We observe the expected behavior, as the curve for $R_b=0.5$ begins at $D=1$, while the curve for $R_b=0.001$ hovers initially near $D=1.722$. Both curves converge at the p_c to the neighborhood of $D=1.89$. The scatter in the data is statistical; each data point is averaged over ten configurations.

IV. SUMMARY

We investigated the breakdown field and the geometry of breakdown paths of an electrical circuit model for dielectric breakdown in media with defects of arbitrary residual resistivity. We investigated the breakdown in an infinite or semi-infinite square lattice with a long needle defect, and breakdown in lattice networks with finite concentrations of random defects.

We found that analytic results from the infinite perfect lattice and percolation theory can help us to understand the breakdown properties of random lattices throughout the concentration range. For defects with nonzero residual resistivity, the breakdown field reaches a finite value as the defects lengthen causing the random lattice to reach the same breakdown field in the thermodynamic limit. We also observed that depending on the initial length of the seed defect and the residual resistivity, the breakdown either grows one dimensionally, or spreads with a fractal dimension. We calculated the phase diagram and relevant exponents for this crossover. A similar spreading crossover also appears in the random lattice with a dilute concentration of defects.

The effects observed in our simulations rely on the unlimited energy supplied by the field source. An open question is how the breakdown field and paths behave when the breakdown is driven by an energy-limited (current-limited) source. This question is also important for practical observation of

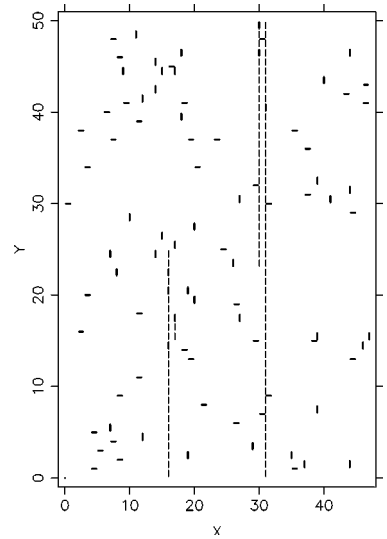

FIG. 13. An example of breakdown paths on a 50×50 lattice with $R_b=0.5$ and $p=0.02$. Thick lines indicate initial defects. The axes X and Y denote the number of lattice spaces in each direction. $D\simeq1$.

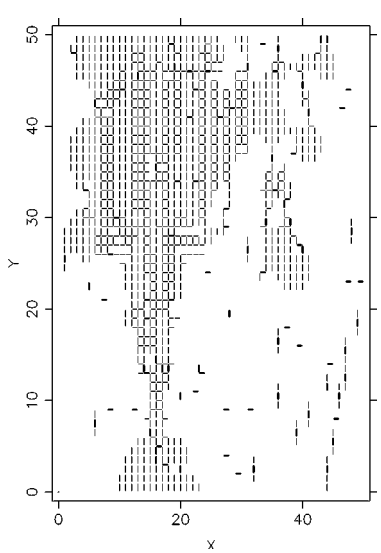

FIG. 12. An example of breakdown paths on 50×50 lattice with $R_b=0.0001$ and $p=0.02$. Thick lines indicate initial defects. The axes X and Y denote the number of lattice spaces in each direction. $D\simeq1.8$.

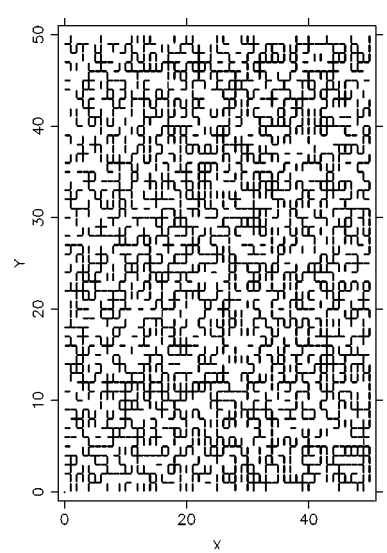

FIG. 14. An example of breakdown paths on a 50×50 lattice with $R_b=0.5$ and $p=0.5$. Thick lines indicate initial defects. The axes X and Y denote the number of lattice spaces in each direction. $D\simeq1.89$.

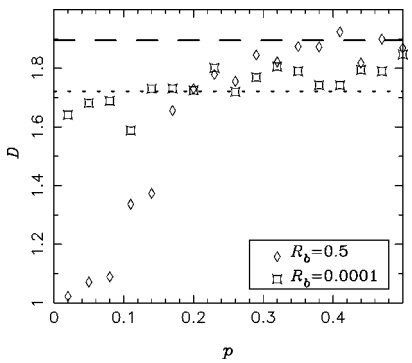

FIG. 15. The fractal dimension D of the largest breakdown cluster vs p plotted for $N=50$. Each point is averaged over ten configurations. The dotted line represents $D=1.722$ for needle growth on an infinite perfect lattice. The dashed line is the fractal dimension of the percolating cluster at $p=p_c$. R_b is the ratio of resistance after breakdown to resistance before breakdown.

these effects, since most adiabatic (i.e., with a very slow voltage rate of rise) dielectric breakdown tests for real applications are performed with strongly current-limited sources.

Also, the effect of open surfaces is very important, as a needle defect near a surface is, due to the image potential, like two neighboring needles in the interior of the sample. This effect was previously noted by Li and Duxbury [4], and recently calculated in a simple fiber-bundle model by Leath and Chen [15]. Future studies should take into account the effect of various boundary conditions.

ACKNOWLEDGMENTS

This research was conducted using the resources of the Cornell Theory Center, which receives major funding from the National Science Foundation (NSF) and New York State, with additional support from the National Center for Research Resources at the National Institutes of Health (NIH), IBM Corporation, and other members of the center's Corporate Partnership Program.

APPENDIX A: ALGORITHM

We wish to compute the field due to n defect bonds, labeled 1 through n, in an otherwise uniform, infinite, perfect, square lattice [Fig. 16(a)]. The basis for the algorithm is the solution for the potential due to a unit current source in an infinite lattice. Consider each defect bond. We can consider it as a parallel combination of the unity lattice resistance and an effective resistance R',

$$\frac{1}{R_b}=1+\frac{1}{R'}, \tag{A1a}$$

$$R'=\frac{R_b}{1-R_b}. \tag{A1b}$$

We can also consider the nodes of this equivalent resistance as a port (terminal pair) of an n-port linear circuit [Fig. 16(b)]. This enables us to use standard electrical circuit theory. The voltage (equal to lattice field) and the current at each port are related by $e_k=-i_kR'$, or, in matrix form, $\overline{e}=-\overline{i}\,R'\,\overline{\overline{I}}$, where $\overline{\overline{I}}$ is the identity matrix.

The voltage e_j at a port j of a linear n-port circuit can be calculated by a linear superposition of voltages produced by the current into each port i_k, and the open-circuit voltage e_j^{oc},

$$e_j=e_j^{\mathrm{oc}}+\sum_{k=1}^{k=n} i_kR_{jk}^{\mathrm{th}}, \tag{A2}$$

or in matrix form

$$\overline{e}=\overline{e}^{\mathrm{oc}}+\overline{i}\,\overline{\overline{R}}^{\mathrm{th}}. \tag{A3}$$

In circuit theory, the proportionality constants R_{jk}^{th} are known as driving-point and transfer resistances (Thévenin equivalent resistances).

The variables are easy to evaluate: the open-circuit voltage e_j^{th} is equal to the applied field E for vertical bonds and zero for horizontal bonds. R_{jk}^{th} is equal to the voltage developed at port j when a unit current source is applied to port k.

The resistance can be found by calculating the voltage due to two unit current sources of opposite polarity attached at the nodes, a dipole source. The solution for this voltage due to a unit current source for a perfect network was evaluated by Watson [16].

Briefly, Watson [16] computed the potential $v(l,m)$ on an infinite lattice of 1-Ω resistances at a distance l horizontal lattice spacings and m vertical lattice spacings from the current source into the lattice at (0,0) by using a discrete form of Laplace equation, namely,

$$4v(m,l)=v(l-1,m)+v(l+1,m)+v(l,m-1)+v(l,m-1)+\delta(l,m). \tag{A4}$$

To find the potential, this equation was Fourier transformed, so that it was possible to solve for the potential, which, when normalized to be zero at the origin, became

$$v(m,l)=\frac{1}{2(2\pi)^2}\int_{-\pi}^{\pi}\int_{-\pi}^{\pi}\frac{dx\,dy(e^{-imx}e^{-ily}-1)}{\cos x+\cos y-2}. \tag{A5}$$

From this result he obtained a set of recursion relations for the potential on the diagonal:

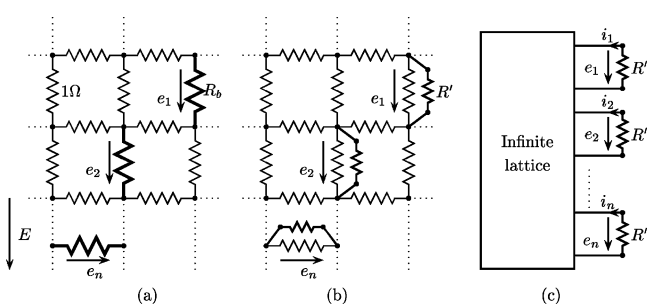

FIG. 16. An infinite lattice network with defect bonds (a), the same lattice with each defect drawn as a parallel combination of resistances (b), and an equivalent electrical n-port network (c).

$$v(m+1,m+1)=\frac{1}{2m+1}[4pv(m,m)-(2m-1)v(m-1,m-1)], \quad \text{(A6)}$$

with

$$v(0,0)=0, \quad v(1,1)=\frac{4}{3\pi}.$$

Also, he obtained a recursion relation for the potential along the principal axes

$$v(0,l)=v(l,0)=\sum_{p=0}^{l-1} I_p, \quad \text{(A7a)}$$

$$I_p=\frac{1}{\pi p}[2+3(2p-1)I_{p-i}-(p-1)I_{p-2}], \quad \text{(A7b)}$$

with

$$I_0=\tfrac{1}{4}, \quad I_1=\frac{2}{\pi}-\frac{3}{4}.$$

The potential at all other nodes can be computed by using Eq. (A4) recursively. Using this procedure, we computed the potential in a 100×100 square due to a single current source at the origin once and for all. To obtain meaningful results, it was necessary to use high-precision arithmetic (120 digits) as the recursion relations are very sensitive to round-off error. Far from the current source, the potential is approximately

$$v(l,m)=\frac{1}{4}+\frac{1}{4\pi}\ln(l^2+m^2). \quad \text{(A8)}$$

We will label by a_{jk} the fraction of the current driven by source j into the bond k. This fraction, which we will call the Watson coefficient, is independent of the nature of the bond, and depends only on the distance and orientation of the bonds. The field in the resistive lattice due to a unit dipole source is then $Ra_{jk}=R_{jk}^{\text{th}}$. Thus, we can find equivalent resistances without having to actually find the equivalent circuit.

Now it is easy to combine this with Eq. (A3) to find the current into each port,

$$\overline{0}=\overline{e^{\text{th}}}+\overline{i}\,(R\overline{\overline{A}}+R'\,\overline{\overline{I}}), \quad \text{(A9)}$$

where $\overline{\overline{A}}$ is the matrix of Watson coefficients. We can solve this equation numerically, for example, by LU decomposition [13]. This algorithm has a number of advantages. It avoids finite-size effects by using an exact solution for an infinite medium. It can easily incorporate perfectly reflecting planes or periodic boundary conditions by methods of images. Also, it is very efficient for small numbers of defects.

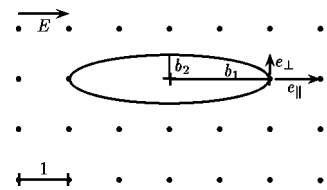

FIG. 17. An elliptical defect as an approximation of a defect cluster on a lattice.

APPENDIX B: ANALYTIC RESULTS FOR ELLIPTICAL DEFECT

We study the fields near an elliptical defect of resistivity ρ_b in a homogeneous continuous medium of resistivity ρ. An elliptical defect represents a continuum approximation to a defect cluster.

To solve the continuum problem, we use elliptical coordinates as described in Morse and Feshbach [17]:

$$x=c\cosh\xi\cos\eta, \quad \text{(B1)}$$

$$y=c\sinh\xi\sin\eta. \quad \text{(B2)}$$

We consider an ellipse with semimajor and minor axes b_1 and b_2, respectively, defined by

$$b_1=c\cosh\xi_0, \quad b_2=c\sinh\xi_0,$$

as shown in Fig. 17.

The applied potential is given by $V=-Ex=-Ec\cosh\xi\cos\eta$. The solution given by Morse and Feshbach [17] for a problem of a dielectric ellipse is easily adapted for the resistive ellipse by associating the resistivity with the dielectric constant.

The potential outside the ellipse takes the form

$$V_o=-Ex+Bce^{-\xi}\cos\eta, \quad \text{(B3)}$$

where

$$B=E\left(1-\frac{\rho_b}{\rho}\right)\frac{e^{\xi_0}\sinh\xi_0\cosh\xi_0}{\frac{\rho_b}{\rho}\cosh\xi_0+\sinh\xi_0}$$
$$=E\left(1-\frac{\rho_b}{\rho}\right)\frac{b_1b_2}{\left(\frac{\rho_b}{\rho}b_1+b_2\right)(b_1-b_2)}. \quad \text{(B4)}$$

To apply the continuum solution to the lattice problem, we express the fields in Cartesian coordinates, and then quantize the field at the lattice spacing, that we take to be unity without loss of generality. Also we normalize the resistance $R_b=\rho_b/\rho$. To convert to Cartesian coordinates, we solve Eq. (B2) for the hyperbolic and trigonometric functions. The result is

$$V_o=-Ex+B\{x-\sqrt{\Delta/2+\sqrt{\Delta^2+4x^2y^2}/2}\}, \quad \text{(B5)}$$

$$\Delta=(x^2-b_1{}^2)-(y^2-b_2{}^2).$$

We can read off the local field e, which is just the difference in potential $V(x,y)$ between adjacent nodes, directly from Eq. (B5). The field at the bond at the tip of the ellipse parallel to the major axis $e_\parallel$ is the voltage difference along the $y=0$ axis:

$$\begin{aligned} e_\parallel &= V_o(b_1,0)-V_o(b_1+1,0) \\ &= E+E(1-R_b)\frac{b_1 b_2}{(R_b b_1+b_2)(b_1-b_2)} \\ &\quad\times\{\sqrt{2b_1+1+b_2{}^2}-b_2-1\}. \end{aligned} \tag{B6a}$$

The tip voltage perpendicular to the major axis of the ellipse is

$$\begin{aligned} e_\perp &= V_o(b_1,0)-V_o(b_1,1)=E(1-R_b)\frac{b_1 b_2}{(R_b b_1+b_2)(b_1-b_2)} \\ &\quad\times\left\{\frac{1}{\sqrt{2}}\sqrt{b_2{}^2-1+\sqrt{(b_2{}^2-1)^2+4b_1{}^2}}-b_2\right\}. \end{aligned} \tag{B7}$$

1. Perfectly conducting defect

A perfectly conducting defect in a material of finite conductivity and a defect of any nonzero conductivity in a perfectly insulating dielectric both have $R_b=0$ and behave identically. The fields at the tip for $b_1 \gg 1$ and $b_1 \gg b_2$ become

$$e_\parallel = E+E\frac{b_1}{(b_1-b_2)}\{\sqrt{2b_1+1+b_2{}^2}-b_2-1\}\sim E+E\sqrt{2b_1}, \tag{B8a}$$

$$\begin{aligned} e_\perp &= E\frac{b_1}{(b_1-b_2)}\left\{\frac{1}{\sqrt{2}}\sqrt{b_2{}^2-1+\sqrt{(b_2{}^2-1)^2+4b_1{}^2}}-b_2\right\} \\ &\sim E\sqrt{b_1}. \end{aligned} \tag{B8b}$$

As the perfectly conducting defect cluster becomes longer, the fields at the tip increase without bounds as the square root of the ellipse length b_1.

2. Defect with nonzero residual resistivity

A similar analysis of Eq. (B5) for $R_b \neq 0$ shows that the fields at the tip first increase with b_1, and then decrease to zero, as was pointed out by Li and Duxbury [4]. However, this behavior is not observed in numerical simulations on lattices. The reason is that as the ellipse becomes longer, the tip becomes very narrow and sharp causing the resistance of the tip to become very large. This makes the ellipse a poor analog for the discrete lattice problem. The resistance of the tip R_{tip} is

$$\begin{aligned} R_{\text{tip}} &= \int_{b_1-1}^{b_1}\rho_b\frac{dx}{b_2\sqrt{1-x^2/b_1{}^2}}=\rho_b\frac{b_1}{b_2}\cos^{-1}\left(1-\frac{1}{b_1}\right) \\ &\sim\frac{\rho_b}{b_2}\sqrt{2b_1}, \end{aligned} \tag{B9}$$

whereas the resistance associated with the lattice element is $\rho_b b_1/b_2$. So, to obtain the correct resistance at the tip, we ''fix'' the width of the ellipse, substituting b_2' for b_2:

$$b_2'=b_1 b_2\cos^{-1}\left(1-\frac{1}{b_1}\right). \tag{B10}$$

Then the asymptotic behavior becomes

$$e_{\parallel\infty}=E[1+2b_2(R_b-1)], \tag{B11a}$$

$$e_{\perp\infty}=Eb_2(R_b-1). \tag{B11b}$$

We see that the field has vastly different behavior for perfectly conducting defects and defects of finite conductivity. For defects of finite conductivity, the fields reach a nonzero asymptotic value.

3. Analytic results for needle defects

The preceding calculation is useful for showing the behavior of arbitrary defect clusters. In this section we develop a more elaborate calculation for an improved understanding of the needle bifurcation. The simple ellipse model has two shortcomings for application to needle growth. The first one is that the numerical coefficients correlate poorly with the exact numerical results on a square lattice. Second, an ellipse is a two-dimensional structure whose representation on a lattice involves resistance changes to bonds that are parallel and perpendicular to the main ellipse axis.

Here we develop a more accurate analytical model. It involves two steps. First, we calculate the fields due to a continuum needle with resistivity R_b by using the ellipse results and taking the limit $b_2\to 0$. However, such fields contain variations on all distance scales, while the fields on a lattice cannot vary at scales greater than $\frac{1}{2}$. Hence it is necessary to filter the resulting field to the appropriate wavelength. To simplify the filtering operation, the continuum fields are expanded in a Taylor series near the tip of the needle, since we are only interested in the fields on bonds adjacent to the needle. The fields are sampled to obtain the voltage at the discrete nodes.

The continuous fields for a needle are

$$e_\parallel=E\sqrt{(x'+b_1)^2-b_1^2}\sim E\left(\sqrt{2b_1x}+\frac{1}{4}\sqrt{\frac{2}{b_1}}x^{3/2}\right), \tag{B12a}$$

$$e_\perp=\frac{E}{\sqrt{2}}\sqrt{-y^2+\sqrt{y^4+4y^2b_1{}^2}}\sim E\left(\sqrt{b_1y}-\frac{1}{4}\sqrt{\frac{1}{b_1}}y^{3/2}\right). \tag{B12b}$$

We take the Laplace transform of the fields using transform pairs $\sqrt{x}\leftrightarrow\frac{1}{2}\sqrt{\pi}s^{-3/2}$ and $x^{3/2}\leftrightarrow\frac{3}{4}\sqrt{\pi}s^{-5/2}$, to obtain

$$e_{\parallel}(s)=E\sqrt{\pi}\left(\sqrt{\frac{b_1}{2}}s^{-3/2}+\frac{3}{16}\sqrt{\frac{2}{b_1}}s^{-5/2}\right), \quad \text{(B13a)}$$

$$e_{\perp}(s)=E\sqrt{\pi}\left(\frac{\sqrt{b_1}}{2}s^{-3/2}-\frac{3}{16}\sqrt{\frac{1}{b_1}}s^{-5/2}\right). \quad \text{(B13b)}$$

For the filter, we a use a single-pole filter $1/[1+(s/\pi)]$. We multiply the fields by the filter and take the inverse transform. We use the following transform pairs:

$$\frac{s^{-3/2}}{1+s/\pi}\leftrightarrow 1/2\pi^{3/2}\left[\frac{x^{3/2}e^{-\pi x}}{(-\pi x)^{3/2}}+2\frac{\sqrt{x}}{\pi^{3/2}}-\frac{x^{3/2}e^{-\pi x}erfc(\sqrt{-\pi x})}{(-\pi x)^{3/2}}\right], \quad \text{(B14a)}$$

$$\frac{s^{-5/2}}{1+s/\pi}\leftrightarrow 3/4\pi^{3/2}\left[\frac{x^{5/2}e^{-\pi x}}{(-\pi x)^{5/2}}+4/3\frac{x^{3/2}}{\pi^{3/2}}-2\frac{\sqrt{x}}{\pi^{5/2}}-\frac{x^{5/2}e^{-\pi x}erfc(\sqrt{-\pi x})}{(-\pi x)^{5/2}}\right]. \quad \text{(B14b)}$$

The field across adjacent bonds is obtained by setting $x=1$ and $y=1$ to obtain the field across the bonds to obtain

$$e_{\parallel}=E\left(1.132\sqrt{b_1}+\frac{0.218}{\sqrt{b_1}}\right), \quad \text{(B15a)}$$

$$e_{\perp}=E\left(0.8\sqrt{b_1}-\frac{0.154}{\sqrt{b_1}}\right). \quad \text{(B15b)}$$

[1] L. A. Dissado, J. Phys. D **23**, 1582 (1990).
[2] P. Duxbury, P. Beale, and P. Leath, Phys. Rev. Lett. **57**, 1052 (1986).
[3] P. Duxbury, P. Beale, and P. Leath, Phys. Rev. B **36**, 367 (1987).
[4] Y. S. Li and P. Duxbury, Phys. Rev. B **36**, 5411 (1987).
[5] Y. S. Li and P. Duxbury, Phys. Rev. B **38**, 9257 (1988).
[6] S. Manna and B. Chakrabarti, Phys. Rev. B **36**, 4078 (1987).
[7] L. Benguigi, Phys. Rev. B **38**, 7211 (1988).
[8] H. Takayasu, Phys. Rev. Lett. **54**, 1099 (1985).
[9] L. Pietronero, A. Erzan, and C. Evertsz, Physica **151**, 207 (1988).
[10] D. Stauffer and A. Aharony, *Introduction to Percolation Theory* (Taylor and Francis, London, 1994).
[11] H. Peitgen, H. Jurgens, and D. Saupe, *Chaos and Fractals* (Springer-Verlag, New York, 1992).
[12] S. Kirkpatrick, Rev. Mod. Phys. **45**, 574 (1973).
[13] W. Press, S. Teukolsky, W. Vetterling, and B. Flannery, *Numerical Recipes in C* (Cambridge University Press, Cambridge, 1992), Chap. 2.
[14] W. Gropp, E. Lusk, and A. Skjellum, *Using MPI* (MIT Press, Cambridge, MA, 1994).
[15] P. Leath and N. Chen, in *Nonlinear Analysis of Fracture*, IUTUM Symposium, edited by J. Willis (Kluwer, Dordrecht, 1997), pp. 265–274.
[16] B. Watson, Ph.D. thesis, Rutgers University, 1975.
[17] P. M. Morse and H. Feshbach, *Methods of Theoretical Physics* (McGraw-Hill, New York, 1953), Part 2, Chap. 10, pp. 1199–1199.